Supplementary Material for Deterministic generation of large-scale hyperentanglement in three degrees of freedom

Xutong Wang[a], Sheng Yu[a], Shengshuai Liu[a], Kai Zhang[a], Yanbo Lou[a], Wei Wang[a], Jietai Jing[a,b,c,d,*]

[a]East China Normal University, School of Physics and Electronic Science, Joint Institute of Advanced Science and Technology, State Key Laboratory of Precision Spectroscopy, Shanghai, China, 200062
[b]CAS Center for Excellence in Ultra-intense Laser Science, Shanghai, China, 201800
[c]Zhejiang University, Department of Physics, Hangzhou, China, 310027
[d]Shanxi University, Collaborative Innovation Center of Extreme Optics, Taiyuan, China, 030006

*Address all correspondence to Jietai Jing, E-mail: jtjing@phy.ecnu.edu.cn

Contents

S1 The fundamental characteristics of Laguerre-Gaussian mode

Laguerre-Gaussian (LG) modes are solutions of the paraxial wave equation. The electric field representation of LG mode in circular-cylindrical coordinate is given by

$$\begin{aligned}\mathrm{LG}_{\ell,p}(r,\phi,z) = \sqrt{\frac{2p!}{\pi(p+|\ell|)!}}\frac{1}{\omega(z)}(\frac{\sqrt{2}r}{\omega(z)})^{|\ell|}\cdot L_p^{|\ell|}(\frac{2r^2}{\omega^2(z)})\cdot exp(-\frac{r^2}{\omega^2(z)}) \\ \cdot exp(i(\ell\phi - \frac{kr^2z}{2(z^2+z_r^2)} + (2p+|\ell|+1)\mathrm{arctan}(\frac{z}{z_r}))),\end{aligned} \tag{S1}$$

where ℓ and p are the azimuthal and radial indexes, respectively; $\omega(z) = \omega(0)\sqrt{1+(z/z_r)^2}$ is the beam waist with $\omega(0)$ being the beam waist at the pupil and $z_r = k\omega^2(0)/2$ being the Rayleigh range; $(2p+|\ell|+1)\mathrm{arctan}(\frac{z}{z_r})$ gives the Gouy phase; $L_p^{|\ell|}(x)$ is the generalized Laguerre polynomial of order p and degree ℓ and can be described as

$$L_p^{|\ell|}(x) = \sum_{k=0}^{p}\frac{(-1)^k(p+|\ell|)!}{k!(p-k)!(|\ell|+k)!}x^k. \tag{S2}$$

The orthogonality between generalized Laguerre polynomial is of the form

$$\int_0^\infty L_{p_1}^{|\ell|}(x)\cdot L_{p_2}^{|\ell|}(x)\cdot x^{|\ell|}e^{-x}dx = \frac{(p_1+|\ell|)!}{p_1!}\delta_{p_1,p_2}, \tag{S3}$$

together with the angular integral

$$\int_0^{2\pi} exp(i(\ell_1-\ell_2)\phi)d\phi = 2\pi\delta_{\ell_1,\ell_2} \tag{S4}$$

resulting in the orthogonality between LG modes

$$\int_0^{2\pi}\int_0^{\infty} \mathrm{LG}_{\ell_1,p_1}(r,\phi)\cdot \mathrm{LG}^{*}_{\ell_2,p_2}(r,\phi) r dr d\phi = \delta_{\ell_1,\ell_2}\delta_{p_1,p_2}. \tag{S5}$$

And it can be seen that azimuthal and radial indexes are independent in mode orthogonality, which indicates that they can form two independent spatial degrees of freedom (DOFs).

S2 The theoretical model

Due to the orbital angular momentum (OAM) conservation, the phase-matching conditions, and the energy conservation respectively, the generated twin modes have the opposite azimuthal quantum number ℓ, the same radial quantum number p, and the opposite frequency shifting from pump beam f under our experimental conditions. Labelling the creation operators of $\mathrm{LG}^{\mathrm{Pr}}_{\ell,p,f}$ and $\mathrm{LG}^{\mathrm{Conj}}_{-\ell,p,-f}$ modes as $\hat{a}^{\dagger}_{\ell,p,f}$ and $\hat{b}^{\dagger}_{-\ell,p,-f}$ respectively and denoting the strength of the interaction with each pair of generated modes as the real parameter $\gamma_{\ell,p,f}$, the interaction Hamiltonian of the four-wave mixing (FWM) process can be written as

$$\hat{H} = \sum_{\ell,p,f} i\hbar\gamma_{\ell,p,f}\hat{a}^{\dagger}_{\ell,p,f}\hat{b}^{\dagger}_{-\ell,p,-f} + \mathrm{H.c.}, \tag{S6}$$

in which $\mathrm{H.c.}$ denotes the Hermitian conjugate. Note that the Hamiltonian is under the "undepleted pump" approximation since the intensity of the pump beam is not significantly changed by the

mixing process. The Hamiltonian can also be written as

$$\begin{aligned}\hat{H} &= \sum_{p,f} i\hbar(\gamma_{0,p,f}\hat{a}^{\dagger}_{0,p,f}\hat{b}^{\dagger}_{0,p,-f} + \gamma_{1,p,f}\hat{a}^{\dagger}_{1,p,f}\hat{b}^{\dagger}_{-1,p,-f} + \gamma_{-1,p,f}\hat{a}^{\dagger}_{-1,p,f}\hat{b}^{\dagger}_{1,p,-f} + \cdots) + \text{H.c.} \\ &= \sum_{\ell,f} i\hbar(\gamma_{\ell,0,f}\hat{a}^{\dagger}_{\ell,0,f}\hat{b}^{\dagger}_{-\ell,0,-f} + \gamma_{\ell,1,f}\hat{a}^{\dagger}_{\ell,1,f}\hat{b}^{\dagger}_{-\ell,1,-f} + \gamma_{\ell,2,f}\hat{a}^{\dagger}_{\ell,2,f}\hat{b}^{\dagger}_{-\ell,2,-f} + \cdots) + \text{H.c.} \\ &= \sum_{\ell,p} i\hbar(\gamma_{\ell,p,f_1}\hat{a}^{\dagger}_{\ell,p,f_1}\hat{b}^{\dagger}_{-\ell,p,-f_1} + \gamma_{\ell,p,f_2}\hat{a}^{\dagger}_{\ell,p,f_2}\hat{b}^{\dagger}_{-\ell,p,-f_2} + \gamma_{\ell,p,f_3}\hat{a}^{\dagger}_{\ell,p,f_3}\hat{b}^{\dagger}_{-\ell,p,-f_3} + \cdots) + \text{H.c.},\end{aligned} \tag{S7}$$

showing that the three independent DOFs are equally important in generating CV hyperentanglement in our system.

Then the corresponding time-evolution operator can be expressed as

$$\hat{U}(t) = e^{-i\hat{H}t/\hbar} = e^{\sum_{\ell,p,f}\gamma_{\ell,p,f}(\hat{a}^{\dagger}_{\ell,p,f}\hat{b}^{\dagger}_{-\ell,p,-f} - \hat{a}_{\ell,p,f}\hat{b}_{-\ell,p,-f})t}. \tag{S8}$$

Using the commutation relations

$$\begin{aligned}[\hat{a}_{\ell_1,p_1,f_1}, \hat{a}^{\dagger}_{\ell_2,p_2,f_2}] = [\hat{b}_{\ell_1,p_1,f_1}, \hat{b}^{\dagger}_{\ell_2,p_2,f_2}] = \delta_{\ell_1,\ell_2}\delta_{p_1,p_2}\delta_{f_1,f_2}, \\ [\hat{a}_{\ell_1,p_1,f_1}, \hat{a}_{\ell_2,p_2,f_2}] = [\hat{a}^{\dagger}_{\ell_1,p_1,f_1}, \hat{a}^{\dagger}_{\ell_2,p_2,f_2}] = [\hat{b}_{\ell_1,p_1,f_1}, \hat{b}_{\ell_2,p_2,f_2}] = [\hat{b}^{\dagger}_{\ell_1,p_1,f_1}, \hat{b}^{\dagger}_{\ell_2,p_2,f_2}] \\ = [\hat{a}_{\ell_1,p_1,f_1}, \hat{b}_{\ell_2,p_2,f_2}] = [\hat{a}^{\dagger}_{\ell_1,p_1,f_1}, \hat{b}^{\dagger}_{\ell_2,p_2,f_2}] = [\hat{a}_{\ell_1,p_1,f_1}, \hat{b}^{\dagger}_{\ell_2,p_2,f_2}] = [\hat{b}_{\ell_1,p_1,f_1}, \hat{a}^{\dagger}_{\ell_2,p_2,f_2}] = 0\end{aligned} \tag{S9}$$

and the Baker-Hasudoff theorem

$$e^{\hat{A}+\hat{B}} = e^{\hat{A}} \cdot e^{\hat{B}} \cdot e^{\frac{1}{2}[\hat{A},\hat{B}]}, \tag{S10}$$

the time-evolution operator can be further written as

$$\hat{U}(t) = e^{\sum_{\ell,p,f} \gamma_{\ell,p,f}(\hat{a}^{\dagger}_{\ell,p,f}\hat{b}^{\dagger}_{-\ell,p,-f} - \hat{a}_{\ell,p,f}\hat{b}_{-\ell,p,-f})t} = \prod_{\ell,p,f} e^{\gamma_{\ell,p,f}(\hat{a}^{\dagger}_{\ell,p,f}\hat{b}^{\dagger}_{-\ell,p,-f} - \hat{a}_{\ell,p,f}\hat{b}_{-\ell,p,-f})t}. \tag{S11}$$

Then by applying the time-evolution operator to the vacuum state, the state of FWM output field can be written as

$$|\psi\rangle_{out} = \hat{U}(t)|vac\rangle = \prod_{\ell,p,f} e^{\gamma_{\ell,p,f}(\hat{a}^{\dagger}_{\ell,p,f}\hat{b}^{\dagger}_{-\ell,p,-f} - \hat{a}_{\ell,p,f}\hat{b}_{-\ell,p,-f})t}|vac\rangle. \tag{S12}$$

Supposing that the mixing interaction occurs over a timescale τ, the time-evolution operator can be described as

$$\hat{U}(\tau) = \prod_{\ell,p,f} e^{\gamma_{\ell,p,f}(\hat{a}^{\dagger}_{\ell,p,f}\hat{b}^{\dagger}_{-\ell,p,-f} - \hat{a}_{\ell,p,f}\hat{b}_{-\ell,p,-f})\tau} = \prod_{\ell,p,f} U_{\ell,p,f}(\tau), \tag{S13}$$

which indicates $\hat{U}(\tau)$ can be applied to a multi-mode vacuum state. Then we set

$$\hat{S}(r_{\ell,p,f}) \equiv \hat{U}_{\ell,p,f}(\tau) = e^{r_{\ell,p,f}(\hat{a}^{\dagger}_{\ell,p,f}\hat{b}^{\dagger}_{-\ell,p,-f} - \hat{a}_{\ell,p,f}\hat{b}_{-\ell,p,-f})}, \tag{S14}$$

which is the so-called two-mode squeezing operator squeezing the modes $\hat{a}_{\ell,p,f}$ and $\hat{b}_{\ell,p,f}$ together; $r_{\ell,p,f} = \gamma_{\ell,p,f}\tau$ is the squeezing parameter quantifying the degree of mixing. Then the final state of FWM output field can be further written as

$$|\psi\rangle_{out} = \prod_{\ell,p,f} \hat{S}(r_{\ell,p,f})|vac\rangle_{\ell,p,f} = \prod_{\ell,p,f} |\psi\rangle_{\ell,p,f}, \tag{S15}$$

where $\hat{S}(r_{\ell,p,f})$ are a series of two-mode squeezing operators corresponding to independent squeezing vacuum states $|\psi\rangle_{\ell,p,f}$ of two modes with the opposite azimuthal quantum number, the same radial quantum number, and the opposite frequency shifting from pump beam.

Each pair of generated modes can be described quantum mechanically by corresponding amplitude and phase quadratures. In our system, they can be written as

$$\begin{aligned} \hat{X}^{\mathrm{Pr}}_{\ell,p,f} = \hat{a}_{\ell,p,f} + \hat{a}^{\dagger}_{\ell,p,f},\ \hat{Y}^{\mathrm{Pr}}_{\ell,p,f} = i(\hat{a}^{\dagger}_{\ell,p,f} - \hat{a}_{\ell,p,f}), \\ \hat{X}^{\mathrm{Conj}}_{-\ell,p,-f} = \hat{b}_{-\ell,p,-f} + \hat{b}^{\dagger}_{-\ell,p,-f},\ \hat{Y}^{\mathrm{Conj}}_{-\ell,p,-f} = i(\hat{b}^{\dagger}_{-\ell,p,-f} - \hat{b}_{-\ell,p,-f}). \end{aligned} \tag{S16}$$

Then we can construct the corresponding covariance matrix σ to characterize the quantum property of each mode pair

$$\sigma = \begin{bmatrix} \langle \hat{X}^{\mathrm{Pr}}_{\ell,p,f}\hat{X}^{\mathrm{Pr}}_{\ell,p,f}\rangle & \langle \hat{X}^{\mathrm{Pr}}_{\ell,p,f}\hat{Y}^{\mathrm{Pr}}_{\ell,p,f}\rangle & \langle \hat{X}^{\mathrm{Pr}}_{\ell,p,f}\hat{X}^{\mathrm{Conj}}_{-\ell,p,-f}\rangle & \langle \hat{X}^{\mathrm{Pr}}_{\ell,p,f}\hat{Y}^{\mathrm{Conj}}_{-\ell,p,-f}\rangle \\ \langle \hat{Y}^{\mathrm{Pr}}_{\ell,p,f}\hat{X}^{\mathrm{Pr}}_{\ell,p,f}\rangle & \langle \hat{Y}^{\mathrm{Pr}}_{\ell,p,f}\hat{Y}^{\mathrm{Pr}}_{\ell,p,f}\rangle & \langle \hat{Y}^{\mathrm{Pr}}_{\ell,p,f}\hat{X}^{\mathrm{Conj}}_{-\ell,p,-f}\rangle & \langle \hat{Y}^{\mathrm{Pr}}_{\ell,p,f}\hat{Y}^{\mathrm{Conj}}_{-\ell,p,-f}\rangle \\ \langle \hat{X}^{\mathrm{Conj}}_{-\ell,p,-f}\hat{X}^{\mathrm{Pr}}_{\ell,p,f}\rangle & \langle \hat{X}^{\mathrm{Conj}}_{-\ell,p,-f}\hat{Y}^{\mathrm{Pr}}_{\ell,p,f}\rangle & \langle \hat{X}^{\mathrm{Conj}}_{-\ell,p,-f}\hat{X}^{\mathrm{Conj}}_{-\ell,p,-f}\rangle & \langle \hat{X}^{\mathrm{Conj}}_{-\ell,p,-f}\hat{Y}^{\mathrm{Conj}}_{-\ell,p,-f}\rangle \\ \langle \hat{Y}^{\mathrm{Conj}}_{-\ell,p,-f}\hat{X}^{\mathrm{Pr}}_{\ell,p,f}\rangle & \langle \hat{Y}^{\mathrm{Conj}}_{-\ell,p,-f}\hat{Y}^{\mathrm{Pr}}_{\ell,p,f}\rangle & \langle \hat{Y}^{\mathrm{Conj}}_{-\ell,p,-f}\hat{X}^{\mathrm{Conj}}_{-\ell,p,-f}\rangle & \langle \hat{Y}^{\mathrm{Conj}}_{-\ell,p,-f}\hat{Y}^{\mathrm{Conj}}_{-\ell,p,-f}\rangle \end{bmatrix}. \tag{S17}$$

According to

$$\hat{S}^{\dagger}(r_{\ell,p,f}) = \hat{S}^{-1}(r_{\ell,p,f}) = \hat{S}(-r_{\ell,p,f}) \tag{S18}$$

and

$$e^{\hat{A}}\hat{B}e^{-\hat{A}} = \sum_{i=0}^{\infty}\frac{1}{i!}[\hat{A}^{(i)}, \hat{B}], \tag{S19}$$

the unitary transformation properties of two-mode squeezing operator can be obtained

$$\begin{aligned}
\hat{S}^{\dagger}(r_{\ell,p,f})\hat{X}^{\mathrm{Pr}}_{\ell,p,f}\hat{S}(r_{\ell,p,f}) &= \hat{X}^{\mathrm{Pr}}_{\ell,p,f}\cosh(r_{\ell,p,f}) + \hat{X}^{\mathrm{Conj}}_{-\ell,p,-f}\sinh(r_{\ell,p,f}),\\
\hat{S}^{\dagger}(r_{\ell,p,f})\hat{X}^{\mathrm{Conj}}_{-\ell,p,-f}\hat{S}(r_{\ell,p,f}) &= \hat{X}^{\mathrm{Conj}}_{-\ell,p,-f}\cosh(r_{\ell,p,f}) + \hat{X}^{\mathrm{Pr}}_{\ell,p,f}\sinh(r_{\ell,p,f}),\\
\hat{S}^{\dagger}(r_{\ell,p,f})\hat{Y}^{\mathrm{Pr}}_{\ell,p,f}\hat{S}(r_{\ell,p,f}) &= \hat{Y}^{\mathrm{Pr}}_{\ell,p,f}\cosh(r_{\ell,p,f}) + \hat{Y}^{\mathrm{Conj}}_{-\ell,p,-f}\sinh(r_{\ell,p,f}),\\
\hat{S}^{\dagger}(r_{\ell,p,f})\hat{Y}^{\mathrm{Conj}}_{-\ell,p,-f}\hat{S}(r_{\ell,p,f}) &= \hat{Y}^{\mathrm{Conj}}_{-\ell,p,-f}\cosh(r_{\ell,p,f}) + \hat{Y}^{\mathrm{Pr}}_{\ell,p,f}\sinh(r_{\ell,p,f}).
\end{aligned} \tag{S20}$$

Then the element of covariance matrix can be calculated

$$\begin{aligned}
\langle \hat{X}^{\mathrm{Pr}}_{\ell,p,f}\hat{X}^{\mathrm{Pr}}_{\ell,p,f}\rangle =& {}_{\ell,p,f}\langle\psi|\hat{X}^{\mathrm{Pr}}_{\ell,p,f}\hat{X}^{\mathrm{Pr}}_{\ell,p,f}|\psi\rangle_{\ell,p,f}\\
=& \langle vac|\hat{S}^{\dagger}(r_{\ell,p,f})\hat{X}^{\mathrm{Pr}}_{\ell,p,f}\hat{S}(r_{\ell,p,f})\hat{S}^{\dagger}(r_{\ell,p,f})\hat{X}^{\mathrm{Pr}}_{\ell,p,f}\hat{S}(r_{\ell,p,f})|vac\rangle = 2G_{\ell,p,f}-1,
\end{aligned} \tag{S21}$$

where $G_{\ell,p,f} = \cosh^2(r_{\ell,p,f})$ is the intensity gain of corresponding mode pair. Similarly all the elements of covariance matrix can be calculated

$$\sigma = \begin{bmatrix}
2G_{\ell,p,f}-1 & 0 & 2\sqrt{G_{\ell,p,f}(G_{\ell,p,f}-1)} & 0\\
0 & 2G_{\ell,p,f}-1 & 0 & -2\sqrt{G_{\ell,p,f}(G_{\ell,p,f}-1)}\\
2\sqrt{G_{\ell,p,f}(G_{\ell,p,f}-1)} & 0 & 2G_{\ell,p,f}-1 & 0\\
0 & -2\sqrt{G_{\ell,p,f}(G_{\ell,p,f}-1)} & 0 & 2G_{\ell,p,f}-1
\end{bmatrix}. \tag{S22}$$

For the purpose of verifying continuous-variable (CV) entanglement, the positivity under partial transposition (PPT) criterion[66] is used. By calculating the smallest symplectic eigenvalue ν of the partially transposed covariance matrix, we can judge whether the state is entangled. If ν is smaller than 1, it is an entangled state; otherwise it is a separable state. In our system, ν can be

written as

$$\begin{aligned}\nu =& min[Eigenvalue(iSM\sigma M)] \\ =& \sqrt{1+8G_{\ell,p,f}(G_{\ell,p,f}-1)-4\sqrt{G_{\ell,p,f}(G_{\ell,p,f}-1)(2G_{\ell,p,f}-1)^2}},\end{aligned} \tag{S23}$$

where

$$S=\begin{bmatrix} 0 & 1 & 0 & 0 \\ -1 & 0 & 0 & 0 \\ 0 & 0 & 0 & 1 \\ 0 & 0 & -1 & 0 \end{bmatrix}, \quad M=\begin{bmatrix} 1 & 0 & 0 & 0 \\ 0 & 1 & 0 & 0 \\ 0 & 0 & 1 & 0 \\ 0 & 0 & 0 & -1 \end{bmatrix}. \tag{S24}$$

It can be seen that ν is smaller than 1 when corresponding $G_{l,p,f}$ is greater than 1, which indicates the existence of CV entanglement. These CV entangled states in three independent DOFs guarantee the generation of large-scale CV hyperentanglement from the FWM process.

S3 Balanced homodyne detection

Balanced homodyne detection (BHD) technique, in which the whole optical field is projected onto a specific mode according to the tailored local oscillator (LO), is widely used in CV system for its high detection efficiency. For BHD, only the signal field with the same frequency as the one of the LO can be extracted. Therefore, in the following calculation, we assume that the signal field and the LO have the same frequency. Regarding LG modes, the BHD scheme is illustrated in Fig. S1. Note that the 50:50 beam splitter (BS) will transform $\mathrm{LG}_{\ell,p,f}$ mode to $\mathrm{LG}_{-\ell,p,f}$ mode when it is get reflected. A LO $\hat{a}\mathrm{LG}_{\ell_1,p_1,f}(r,\phi)$ and a signal field $\hat{b}\mathrm{LG}_{\ell_2,p_2,f}(r,\phi)$ are incident into the two ports

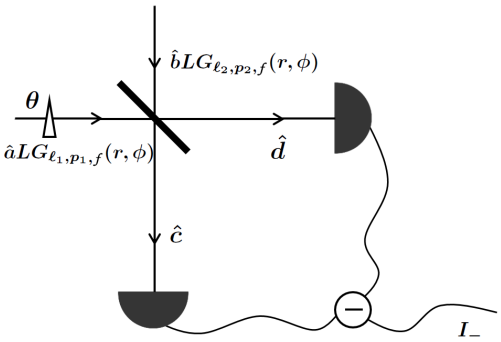

Fig S1 Schematic of balanced homodyne detection. A local oscillator and a signal field are incident into the two ports of a 50:50 beam splitter, then the fields of two output ports are measured by two detectors whose photocurrents are subtracted by a subtractor.

of a BS respectively, then the fields of two output ports can be written as

$$\begin{aligned}\hat{c} &= \frac{1}{\sqrt{2}}[\hat{a}\mathrm{LG}_{-\ell_1,p_1,f}(r,\phi)\cdot e^{i\theta} + \hat{b}\mathrm{LG}_{\ell_2,p_2,f}(r,\phi)],\\ \hat{d} &= \frac{1}{\sqrt{2}}[\hat{a}\mathrm{LG}_{\ell_1,p_1,f}(r,\phi)\cdot e^{i\theta} - \hat{b}\mathrm{LG}_{-\ell_2,p_2,f}(r,\phi)],\end{aligned} \tag{S25}$$

where θ is the relative phase difference between LO and signal field. Then the fields $\hat{c}$ and $\hat{d}$ are detected, after which the two detected photocurrents are subtracted by a subtractor. The difference photocurrent can be expressed as

$$\begin{aligned}I_- &= \int_0^{2\pi}\int_0^{\infty}(\hat{d}^\dagger\hat{d} - \hat{c}^\dagger\hat{c})rdrd\phi\\ &\propto \int_0^{\infty}(\frac{\sqrt{2}r}{\omega})^{|\ell_1|}(\frac{\sqrt{2}r}{\omega})^{|\ell_2|}\cdot L_{p_1}^{|\ell_1|}(\frac{2r^2}{\omega^2})\cdot L_{p_2}^{|\ell_2|}(\frac{2r^2}{\omega^2})\cdot exp(-\frac{2r^2}{\omega^2})rdr\\ &\quad\cdot\int_0^{2\pi}\frac{1}{2}[\hat{a}^\dagger\hat{b}e^{-i(\ell_1+\ell_2)\phi}e^{-i\theta} + \hat{b}^\dagger\hat{a}e^{i(\ell_1+\ell_2)\phi}e^{i\theta} + \hat{a}^\dagger\hat{b}e^{i(\ell_1+\ell_2)\phi}e^{-i\theta} + \hat{b}^\dagger\hat{a}e^{-i(\ell_1+\ell_2)\phi}e^{i\theta}]d\phi.\end{aligned} \tag{S26}$$

We express $\hat{a}$ and $\hat{b}$ as

$$\begin{aligned}\hat{a} &\approx |\alpha| + \delta\hat{a} \\ \hat{b} &\approx |\beta| + \delta\hat{b}\end{aligned} \tag{S27}$$

and neglect terms without $|\alpha|$ because the coherence amplitude of the LO is much larger than that of the signal field ($|\alpha| \gg |\beta|$). Then the difference photocurrent can be approximated as

$$\begin{aligned} I_- &\propto \int_0^\infty (\frac{\sqrt{2}r}{\omega})^{|\ell_1|}(\frac{\sqrt{2}r}{\omega})^{|\ell_2|} \cdot L_{p_1}^{|\ell_1|}(\frac{2r^2}{\omega^2}) \cdot L_{p_2}^{|\ell_2|}(\frac{2r^2}{\omega^2}) \cdot exp(-\frac{2r^2}{\omega^2}) r dr \cdot \int_0^{2\pi} |\alpha| \cos[(\ell_1+\ell_2)\phi] \delta X_b^\theta d\phi \\ &\propto |\alpha| \delta X_b^\theta \delta_{l_1,-l_2} \delta_{p_1,p_2} \end{aligned}, \tag{S28}$$

where $\delta X_b^\theta = \delta b e^{-i\theta} + \delta\hat{b}^\dagger e^{i\theta}$ is the amplitude quadrature of the signal field. It can be seen that the difference photocurrent is proportional to the quantum fluctuation of a specific LG mode which has the opposite azimuthal index and the same radial index as the LO.

S4 Measurement of covariance matrix

In our experiment, the probe and conjugate beam are detected by two sets of BHD respectively. Then the normalized diagonal terms of covariance matrix can be obtained by

$$\begin{aligned} \langle \hat{X}_{\ell,p,f}^{\mathrm{Pr}} \hat{X}_{\ell,p,f}^{\mathrm{Pr}} \rangle &= \frac{\Delta^2(L_{-\ell,p,f}^{\mathrm{Pr}} \hat{X}_{\ell,p,f}^{\mathrm{Pr}})}{\Delta^2(L_{-\ell,p,f}^{\mathrm{Pr}} \hat{X}_{vac})}, \quad \langle \hat{Y}_{\ell,p,f}^{\mathrm{Pr}} \hat{Y}_{\ell,p,f}^{\mathrm{Pr}} \rangle = \frac{\Delta^2(L_{-\ell,p,f}^{\mathrm{Pr}} \hat{Y}_{\ell,p,f}^{\mathrm{Pr}})}{\Delta^2(L_{-\ell,p,f}^{\mathrm{Pr}} \hat{Y}_{vac})} \\ \langle \hat{X}_{-\ell,p,-f}^{\mathrm{Conj}} \hat{X}_{-\ell,p,-f}^{\mathrm{Conj}} \rangle &= \frac{\Delta^2(L_{\ell,p,-f}^{\mathrm{Conj}} \hat{X}_{-\ell,p,-f}^{\mathrm{Conj}})}{\Delta^2(L_{\ell,p,-f}^{\mathrm{Conj}} \hat{X}_{vac})}, \quad \langle \hat{Y}_{-\ell,p,-f}^{\mathrm{Conj}} \hat{Y}_{-\ell,p,-f}^{\mathrm{Conj}} \rangle = \frac{\Delta^2(L_{\ell,p,-f}^{\mathrm{Conj}} \hat{Y}_{-\ell,p,-f}^{\mathrm{Conj}})}{\Delta^2(L_{\ell,p,-f}^{\mathrm{Conj}} \hat{Y}_{vac})}, \end{aligned} \tag{S29}$$

where $\hat{X}^{\mathrm{Pr}}_{\ell,p,f}$ ($\hat{X}^{\mathrm{Conj}}_{-\ell,p,-f}$), $\hat{Y}^{\mathrm{Pr}}_{\ell,p,f}$ ($\hat{Y}^{\mathrm{Conj}}_{-\ell,p,-f}$) are the amplitude quadrature and phase quadrature of probe (conjugate) beam, respectively, $L^{\mathrm{Pr}}_{-\ell,p,f}$ ($L^{\mathrm{Conj}}_{\ell,p,-f}$) is the optical power of LO, $\Delta^2(L^{\mathrm{Pr}}_{-\ell,p,f}\hat{X}^{\mathrm{Pr}}_{\ell,p,f})$ ($\Delta^2(L^{\mathrm{Conj}}_{\ell,p,-f}\hat{X}^{\mathrm{Conj}}_{-\ell,p,-f})$) is the noise power of photocurrent when the signal field is fed into the detectors, and $\Delta^2(L^{\mathrm{Pr}}_{-\ell,p,f}\hat{X}_{vac})$ ($\Delta^2(L^{\mathrm{Conj}}_{\ell,p,-f}\hat{Y}_{vac})$) is the noise power of photocurrent when the signal field is blocked. By combining the photocurrents of two BHDs via a adder (subtractor), we can measure the noise power of the sum (difference) of the two photocurrents, and the minimum of the measurement result is equal to $\Delta^2(L^{\mathrm{Pr}}_{-\ell,p,f}\hat{Y}^{\mathrm{Pr}}_{\ell,p,f} + L^{\mathrm{Conj}}_{\ell,p,-f}\hat{Y}^{\mathrm{Conj}}_{-\ell,p,-f})$ ($\Delta^2(L^{\mathrm{Pr}}_{-\ell,p,f}\hat{X}^{\mathrm{Pr}}_{\ell,p,f} - L^{\mathrm{Conj}}_{\ell,p,-f}\hat{X}^{\mathrm{Conj}}_{-\ell,p,-f})$). Then we can obtain

$$\langle \hat{X}^{\mathrm{Pr}}_{\ell,p,f}\hat{X}^{\mathrm{Conj}}_{-\ell,p,-f}\rangle = \frac{\Delta^2(L^{\mathrm{Pr}}_{-\ell,p,f}\hat{X}^{\mathrm{Pr}}_{\ell,p,f}) + \Delta^2(L^{\mathrm{Conj}}_{\ell,p,-f}\hat{X}^{\mathrm{Conj}}_{-\ell,p,-f}) - \Delta^2(L^{\mathrm{Pr}}_{-\ell,p,f}\hat{X}^{\mathrm{Pr}}_{\ell,p,f} - L^{\mathrm{Conj}}_{\ell,p,-f}\hat{X}^{\mathrm{Conj}}_{-\ell,p,-f})}{2\sqrt{\Delta^2(L^{\mathrm{Pr}}_{-\ell,p,f}\hat{X}_{vac})}\sqrt{\Delta^2(L^{\mathrm{Conj}}_{\ell,p,-f}\hat{X}_{vac})}} \tag{S30}$$

In a similar way, all the normalized off-diagonal terms of the covariance matrix can be obtained. Then we can fully construct the covariance matrix for characterizing the CV hyperentanglement.

S5 Frequency bandwidth for maintaining entanglement

The frequencies of generated probe and conjugate beams from our system are tunable. In our experiment, the frequency of seeded probe beam is redshifted from the pump beam frequency through an acousto-optic modulator (AOM). By changing the input radio-frequency signal of the AOM, we can set the frequency shifting f of the probe beam. In this way, probe (conjugate) beam with a frequency of $\omega_{\mathrm{Pump}} - f$ ($\omega_{\mathrm{Pump}} + f$) is generated from the FWM process, where $\omega_{\mathrm{Pump}} = 377.1102$ THz is the frequency of pump beam. Such probe and conjugate beams are used for LOs of the two BHDs to extract corresponding frequency mode from the unseeded FWM process. Then we do a series of entanglement measurements between $\mathrm{LG}^{\mathrm{Pr}}_{3,2,f}$ and $\mathrm{LG}^{\mathrm{Conj}}_{-3,2,-f}$ modes

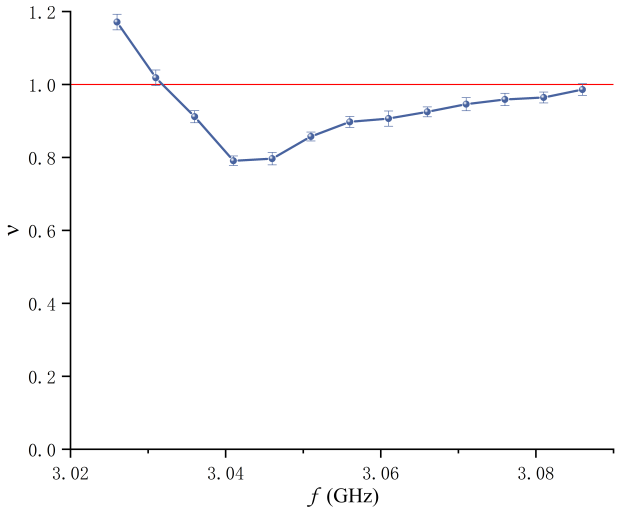

Fig S2 The smallest symplectic eigenvalue ν for $\mathrm{LG}^{\mathrm{Pr}}_{3,2,f}$ and $\mathrm{LG}^{\mathrm{Conj}}_{-3,2,-f}$ modes as a function of f. The error bars are obtained from the standard deviations of multiple repeated measurements.

with varying f. The smallest symplectic eigenvalue ν as a function of f is shown in Fig. S2. As can be seen, for f in a range of about 55 MHz, ν is always smaller than one, indicating the existence of CV entanglement. Therefore, for maintaining entanglement, the frequency bandwidth of our system for the case of $\ell = 3$ and $p = 2$ is about 55 MHz. The frequency bandwidth for arbitrary LG modes can be measured in a similar way. They are all at the level of tens of MHz.

S6 Independent addressability of entangled frequency modes

The detailed experimental setup confirming that the generated frequency modes will not mix and can be independently addressed is shown in Fig. S3, where two seeded and an unseeded FWM processes happen in the same ^{85}Rb vapor cell. The frequency-multiplexed CV entanglement is generated from the unseeded FWM process (inside the dashed frame), while the two seeded FWM processes are used for generating respective LOs of the two BHDs. A cavity stabilized Ti:sapphire laser produces a beam whose frequency is around 377.1102 THz (ω_{Pump}). The beam is divided into three, one of which is further split, serving as respective pump beams of the three FWM processes.

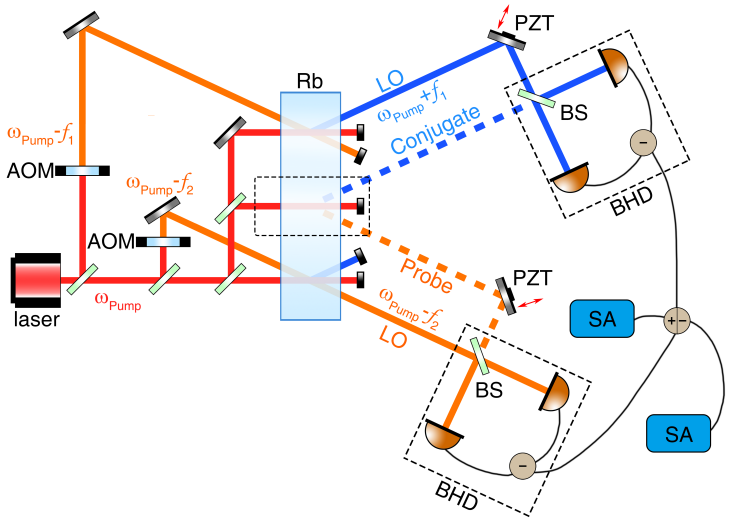

Fig S3 Experimental setup for independently addressing different frequency modes.

The other two beams are redshifted by f_1 and f_2, respectively, through two AOMs, serving as respective seeding probe beams of the two seeded FWM processes. Due to the energy conservation, bright beams with frequency sideband modes $\omega_{\mathrm{Pump}} \pm f_1$ and $\omega_{\mathrm{Pump}} \pm f_2$ are generated from the two seeded FWM processes, respectively. In order to measure the covariance matrix elements, two BHDs are employed. One for detecting probe beam and the other one for detecting conjugate beam. The generated fields from the unseeded FWM process will be projected onto the same frequency mode with the LOs, which ensures the perfect extraction of the desired frequency mode in the BHD. We choose two bright beams generated from the seeded FWM processes, $\omega_{\mathrm{Pump}} + f_1$ and $\omega_{\mathrm{Pump}} - f_2$, as the respective LOs of the two BHDs. In this way, the probe (conjugate) field will be projected onto $\omega_{\mathrm{Pump}} - f_2$ ($\omega_{\mathrm{Pump}} + f_1$) mode. The photocurrents from the two BHDs together with their subtraction and addition are recorded by the spectrum analyzers (SAs). Then we can obtain the variances of amplitude quadrature $\hat{X}^{\mathrm{Pr}}_{f_2}$ ($\hat{X}^{\mathrm{Conj}}_{-f_1}$) and phase quadrature $\hat{Y}^{\mathrm{Pr}}_{f_2}$ ($\hat{Y}^{\mathrm{Conj}}_{-f_1}$) of the probe (conjugate) beam and the covariance of two-beam quadratures.

As mentioned above, in the BHDs, the probe field will be projected onto $\omega_{\mathrm{Pump}} - f_2$ mode,

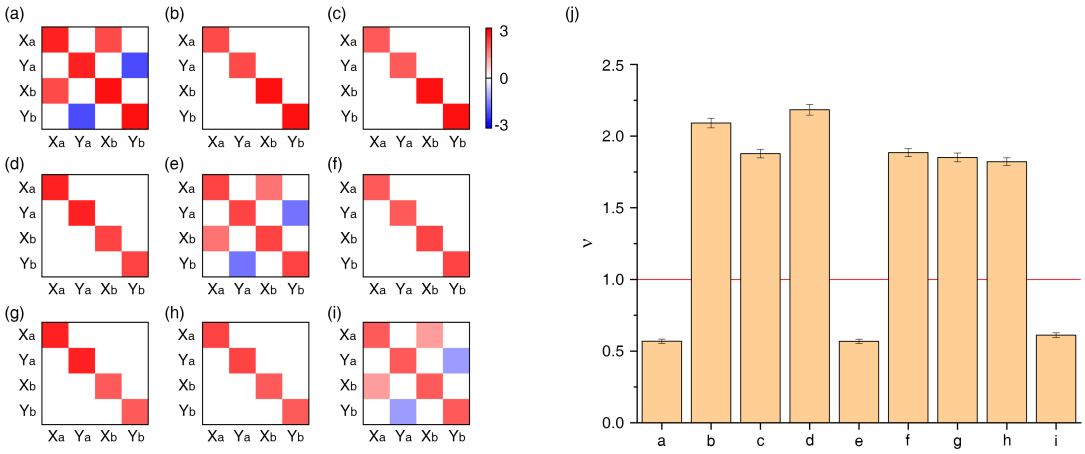

Fig S4 Experimentally measured covariance matrices between frequency modes (a) ω_{Pump}-3.04 GHz and ω_{Pump}+3.04 GHz, (b) ω_{Pump}-3.045 GHz and ω_{Pump}+3.04 GHz, (c) ω_{Pump}-3.05 GHz and ω_{Pump}+3.04 GHz, (d) ω_{Pump}-3.04 GHz and ω_{Pump}+3.045 GHz, (e) ω_{Pump}-3.045 GHz and ω_{Pump}+3.045 GHz, (f) ω_{Pump}-3.05 GHz and ω_{Pump}+3.045 GHz, (g) ω_{Pump}-3.04 GHz and ω_{Pump}+3.05 GHz, (h) ω_{Pump}-3.045 GHz and ω_{Pump}+3.05 GHz, (i) ω_{Pump}-3.05 GHz and ω_{Pump}+3.05 GHz. (j) The corresponding smallest symplectic eigenvalues of partially transposed covariance matrices between different frequency modes.

while the conjugate field will be projected onto $\omega_{\mathrm{Pump}} + f_1$ mode. We perform measurements of the covariance matrix between frequency modes $\omega_{\mathrm{Pump}} - f_2$ and $\omega_{\mathrm{Pump}} + f_1$ by changing the amounts of frequency shift f_1 and f_2 with $f_1, f_1 \in \{3.04\ \mathrm{GHz}, 3.045\ \mathrm{GHz}, 3.05\ \mathrm{GHz}\}$. The nine experimentally measured covariance matrices are shown in Figs. S4(a)-S4(i). As can be seen from Figs. S4(a), S4(e), and S4(i), for the three frequency sidebands satisfying energy conservation ($f_1 = f_2$), the correlations of $\hat{X}^{\mathrm{Pr}}_{f_2}$,$\hat{X}^{\mathrm{Conj}}_{-f_1}$ and anticorrelations of $\hat{Y}^{\mathrm{Pr}}_{f_2}$,$\hat{Y}^{\mathrm{Conj}}_{-f_1}$ are apparent in the off-diagonal elements of the covariance matrices. The corresponding smallest symplectic eigenvalues of partially transposed covariance matrices are smaller than one, as shown in Fig. S4(j), which verifies the CV entanglement between two correlated frequency modes. In contrast, as shown in Figs. S4(b), S4(c), S4(d), S4(f), S4(g), and S4(h), for frequency modes that do not satisfy energy conservation ($f_1 \neq f_2$), all the off-diagonal elements of covariance matrices are around zero, showing no correlations between the frequency modes. Accordingly, the smallest symplectic

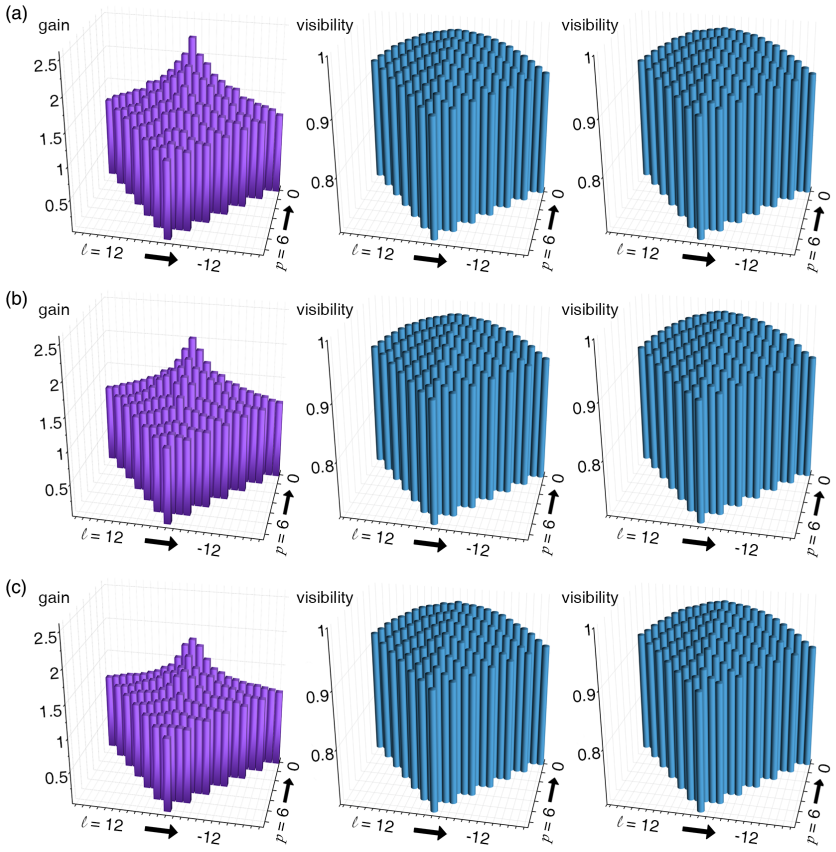

Fig S5 (From left to right) Intensity gain, interference visibility of the BHD for detecting the probe beam, and interference visibility of the BHD for detecting the conjugate beam as a function of the two quantum numbers ℓ and p at different frequency in the case of (a) $f = 3.04$ GHz, (b) $f = 3.045$ GHz, and (c) $f = 3.05$ GHz, respectively.

eigenvalues of partially transposed covariance matrices are all above one, certifying the separability between uncorrelated frequency modes. Our results clearly show that the frequency sidebands spaced by 5 MHz are independently generated from the FWM process and can be independently addressed by BHD. Therefore, frequency can be characterized as a potential multiplexing resource in our system.

S7 The intensity gain of the FWM process and the interference visibility of BHD

For the purpose of testing the intensity gain of the FWM, we switch the unseeded FWM process to the seeded process by seeding a bright probe beam of $\mathrm{LG}_{\ell,p,f}$. In this way, the intensity gains

varying with ℓ, p, and f are shown in each subfigure of Fig. S5 (left). It can be seen that the higher the LG mode order is, the smaller the intensity gain will be, which is in consequence of the beam size increase of higher-order LG modes. Such increment in beam size results in the reduced overlap with the pump beam and thus weaker nonlinear interaction strength. By making the two FWM interactions identical, we can record the interference visibilities between the corresponding LO and probe (conjugate) fields, which is illustrated in the middle (right) of each subfigure of Fig. S5. These visibilities are within the range of 0.90 and 0.98 and decrease slightly with the increasing of the mode order, indicating the BHD extraction efficiency for different LG modes.

S8 Theoretical prediction for the experimental results

To estimate the possible number of entangled spatial modes, we refer to the Schmidt number[67] which is roughly the number of pairs of optical modes coupled in the gain region.[68] For our system, in the ideal case (without any losses and noises introduced) the generated twin modes are entangled as long as the corresponding gain is greater than one (Eq. S23). Therefore, the possible number of pairs of entangled spatial modes is equal to the number of pairs of optical modes coupled in the gain region, i.e., the Schmidt number.

The Schmidt decomposition of the two-photon field is equivalent to a coherent mode decomposition of the coherence function of the reduced one-photon field. The reduced one-photon field is an incoherent mixture of all of the Schmidt modes. The Schmidt number can thus be estimated according to the one-photon coherence of the FWM emission. In our system, the Schmidt number K can be calculated by

$$K = (\frac{w_p}{w_{coh}})^2, \tag{S31}$$

which counts the number of independent coherent regions in the source,[68,69] where w_p is the pump beam waist, w_{coh} is the transverse coherence width, i.e. the waist of a beam such that the Rayleigh range is equal to the length of the gain medium, which can be calculated from $w_{coh} = \sqrt{L\lambda/n\pi}$. In our experiment, the waist of pump beam w_p is about 950 μm, the cell length L is 12 mm, the wavelength λ is 795 nm, and the refractive index n is 1. Therefore, we get $K \approx 297$. In other words, there are about 297 Schmidt modes available in our system in the ideal case.

However, the number of experimentally accessible entangled mode pairs is lower than the theoretically predicted Schmidt number. This is due to the fact that CV entanglement is very sensitive to losses and noises, and the degree of CV entanglement is affected by the imperfections of the experiment.[5] Various imperfections, such as atomic absorption, propagation losses, imperfect homodyne visibilities, non-unity quantum efficiency of photodiode, and scattered pump light, are unavoidable in our experiment, which introduce excess noise and deteriorate the entanglement. Meanwhile, higher-order spatial modes have less overlap with the pump beam, resulting in smaller gain and thus smaller degree of CV entanglement. In our experiment, the entanglement between high-order LG modes disappears due to the excess noise and too small gain. To better predict the experimental results considering the experimental imperfections, we use a theoretical model for gain, loss, and noise in the measurement of CV hyperentanglement.

The optical losses caused by atomic absorption, light propagation, and photodiode can be modeled by optical beam splitters (BS1 and BS2), which combine signal field with extra vacuum field ($\hat{a}_v$ for probe and $\hat{b}_v$ for conjugate), placed in the beam paths as shown in Fig. S6. The transmittance of probe (conjugate) field is $\eta_a = \eta_{a1}\eta_{a2}\eta_{a3}$ ($\eta_b = \eta_{b1}\eta_{b2}\eta_{b3}$), where $\eta_{a1} = 0.88$ ($\eta_{b1} = 0.95$) is the transmittance for probe (conjugate) beam in atomic vapor cell, $\eta_{a2} = 0.95$ ($\eta_{b2} = 0.94$) is the transmission efficiency of probe (conjugate) beam during propagation, $\eta_{a3} = 0.85$ ($\eta_{b3} = 0.85$)

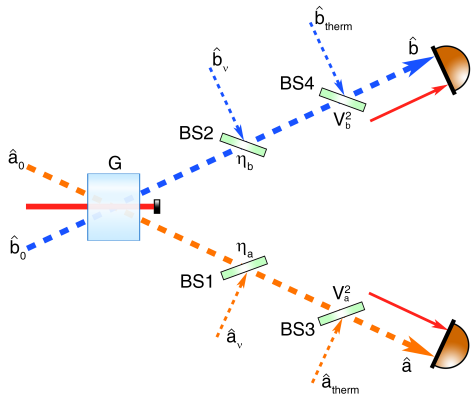

Fig S6 The theoretical model for gain, loss, and noise in the measurement of CV hyperentanglement.

is the quantum efficiency of photodiode (Hamamatsu S5972). Meanwhile, imperfect homodyne visibilities will lead to increased losses and then uncorrelated noise, which will deteriorate the entanglement. For our multi-spatial-mode system, imperfect homodyne visibilities can couple in uncorrelated amplified modes, and hence can cause larger degradation of the measured squeezing than the single-mode system where homodyne mismatch introduces only the vacuum noise. We model the effect of imperfect visibilities of balanced homodyne detections (BHDs) with optical beam splitters (BS3 and BS4) whose transmittances are V_a^2 and V_b^2 for probe and conjugate beams, where V_a and V_b are the visibilities of the BHDs for detecting the probe and conjugate beams respectively. To account for the coupling of uncorrelated amplified modes due to the mode mismatch of our BHDs, we couple in uncorrelated thermal fields ($\hat{a}_{therm}$ for probe and $\hat{b}_{therm}$ for conjugate), which have noise power equal to those of the signal fields, through the second ports of beam splitters BS3 and BS4. In addition, the scattered pump light will be detected by the photodiode and thus introduce excess noise to this system.

The input-output relations of our system with considering atomic absorption, propagation losses, imperfect homodyne visibilities, and non-unity quantum efficiency of photodiode can be

written as

$$\begin{aligned}\hat{a} &= V_a\sqrt{\eta_a G}\hat{a}_0 + V_a\sqrt{\eta_a(G-1)}\hat{b}_0^\dagger + \sqrt{\eta_a(1-V_a^2)}\hat{a}_{therm} + \sqrt{1-\eta_a}\hat{a}_v,\\ \hat{b} &= V_b\sqrt{\eta_b G}\hat{b}_0 + V_b\sqrt{\eta_b(G-1)}\hat{a}_0^\dagger + \sqrt{\eta_b(1-V_b^2)}\hat{b}_{therm} + \sqrt{1-\eta_b}\hat{b}_v,\end{aligned} \tag{S32}$$

where G is the intensity gain of the unseeded FWM process, $\hat{a}$ ($\hat{b}$) is the detected probe (conjugate) field, as shown in Fig. S6. The quantum properties of generated probe and conjugate fields can be described by corresponding amplitude and phase quadratures. In our system, they can be written as

$$\hat{X}_a = \hat{a} + \hat{a}^\dagger, \hat{Y}_a = i(\hat{a}^\dagger - \hat{a}), \hat{X}_b = \hat{b} + \hat{b}^\dagger, \hat{Y}_b = i(\hat{b}^\dagger - \hat{b}). \tag{S33}$$

Then the variances and covariances of the probe ($\hat{a}$) and conjugate ($\hat{b}$) fields can be calculated as

$$\begin{aligned}\Delta^2(\hat{X}_a) = \Delta^2(\hat{Y}_a) &= 2\eta_a(G-1)+1,\\ \Delta^2(\hat{X}_b) = \Delta^2(\hat{Y}_b) &= 2\eta_b(G-1)+1,\\ Cov(\hat{X}_a,\hat{X}_b) &= 2V_aV_b\sqrt{\eta_a\eta_b G(G-1)},\\ Cov(\hat{Y}_a,\hat{Y}_b) &= -2V_aV_b\sqrt{\eta_a\eta_b G(G-1)},\\ Cov(\hat{X}_a,\hat{Y}_a) = Cov(\hat{X}_a,\hat{Y}_b) &= Cov(\hat{X}_b,\hat{Y}_b) = Cov(\hat{X}_b,\hat{Y}_a) = 0.\end{aligned} \tag{S34}$$

In the practical measurements of covariance matrix, the detected matrix elements are obtained by the variances of photocurrents from BHDs with considering the detected signal field and scattered

pump light

$$
\begin{aligned}
\langle \hat{X}_a \hat{X}_a \rangle =& \frac{\Delta^2(L_a\hat{X}_a + P_{c1}\hat{X}_{c1} + P_{c2}\hat{X}_{c2})}{\Delta^2(L_a\hat{X}_{vac} + P_{c2}\hat{X}_{c2})} = \frac{L_a^2}{L_a^2 + P_{c2}^2}(2\eta_a(G-1)+1) + \frac{P_{c1}^2 + P_{c2}^2}{L_a^2 + P_{c2}^2}, \\
\langle \hat{X}_a \hat{X}_b \rangle =& \frac{\Delta^2(L_a\hat{X}_a + P_{c1}\hat{X}_{c1} + P_{c2}\hat{X}_{c2}) + \Delta^2(L_b\hat{X}_b + P_{c3}\hat{X}_{c3} + P_{c4}\hat{X}_{c4})}{2\sqrt{\Delta^2(L_a\hat{X}_{vac} + P_{c2}\hat{X}_{c2})}\sqrt{\Delta^2(L_b\hat{X}_{vac} + P_{c4}\hat{X}_{c4})}} \\
& - \frac{\Delta^2((L_a\hat{X}_a + P_{c1}\hat{X}_{c1} + P_{c2}\hat{X}_{c2}) - (L_b\hat{X}_b + P_{c2}\hat{X}_{c2} + P_{c4}\hat{X}_{c4}))}{2\sqrt{\Delta^2(L_a\hat{X}_{vac} + P_{c2}\hat{X}_{c2})}\sqrt{\Delta^2(L_b\hat{X}_{vac} + P_{c4}\hat{X}_{c4})}} \\
=& \frac{2V_aV_b\sqrt{\eta_a\eta_b G(G-1)}}{\sqrt{1+(P_{c2}/L_a)^2}\sqrt{1+(P_{c4}/L_b)^2}},
\end{aligned}
\tag{S35}
$$

where L_a and L_b are the optical powers of LOs for detecting the probe and conjugate fields which are equal to GI_0 and $(G-1)I_0$, respectively, because the LOs are generated by a similar FWM process with the aforementioned unseeded FWM process, and I_0 is the optical power of the seeding probe beam. P_{c1} (P_{c3}) and P_{c2} (P_{c4}), whose values are estimated to about $0.12I_0$, are the optical power of scattered pump light, incident on the probe (conjugate) homodyne detector, of the seeded and unseeded FWM, and $\hat{X}_{c1}$ ($\hat{X}_{c3}$) and $\hat{X}_{c2}$ ($\hat{X}_{c4}$) are the corresponding quadratures of scattered pump light detected by the photodiode which are assumed to have the noise level of vacuum state. Similarly, all the covariance matrix elements are obtained

$$
\begin{aligned}
\langle \hat{X}_a \hat{X}_a \rangle = \langle \hat{Y}_a \hat{Y}_a \rangle =& \frac{G^2}{G^2 + 0.12^2}(2\eta_a(G-1)+1) + \frac{2\times 0.12^2}{G^2+0.12^2}, \\
\langle \hat{X}_b \hat{X}_b \rangle = \langle \hat{Y}_b \hat{Y}_b \rangle =& \frac{(G-1)^2}{(G-1)^2 + 0.12^2}(2\eta_a(G-1)+1) + \frac{2\times 0.12^2}{(G-1)^2+0.12^2}, \\
\langle \hat{X}_a \hat{X}_b \rangle = \langle \hat{X}_b \hat{X}_a \rangle =& \frac{2V_aV_b\sqrt{\eta_a\eta_b G(G-1)}}{\sqrt{1+(0.12/G)^2}\sqrt{1+(0.12/(G-1))^2}}, \\
\langle \hat{Y}_a \hat{Y}_b \rangle = \langle \hat{Y}_b \hat{Y}_a \rangle =& -\frac{2V_aV_b\sqrt{\eta_a\eta_b G(G-1)}}{\sqrt{1+(0.12/G)^2}\sqrt{1+(0.12/(G-1))^2}}, \\
\langle \hat{X}_a \hat{Y}_a \rangle = \langle \hat{X}_a \hat{Y}_b \rangle =& \langle \hat{Y}_a \hat{X}_a \rangle = \langle \hat{Y}_a \hat{X}_b \rangle = \langle \hat{X}_b \hat{Y}_a \rangle = \langle \hat{X}_b \hat{Y}_b \rangle = \langle \hat{Y}_b \hat{X}_a \rangle = \langle \hat{Y}_b \hat{X}_b \rangle = 0.
\end{aligned}
\tag{S36}
$$

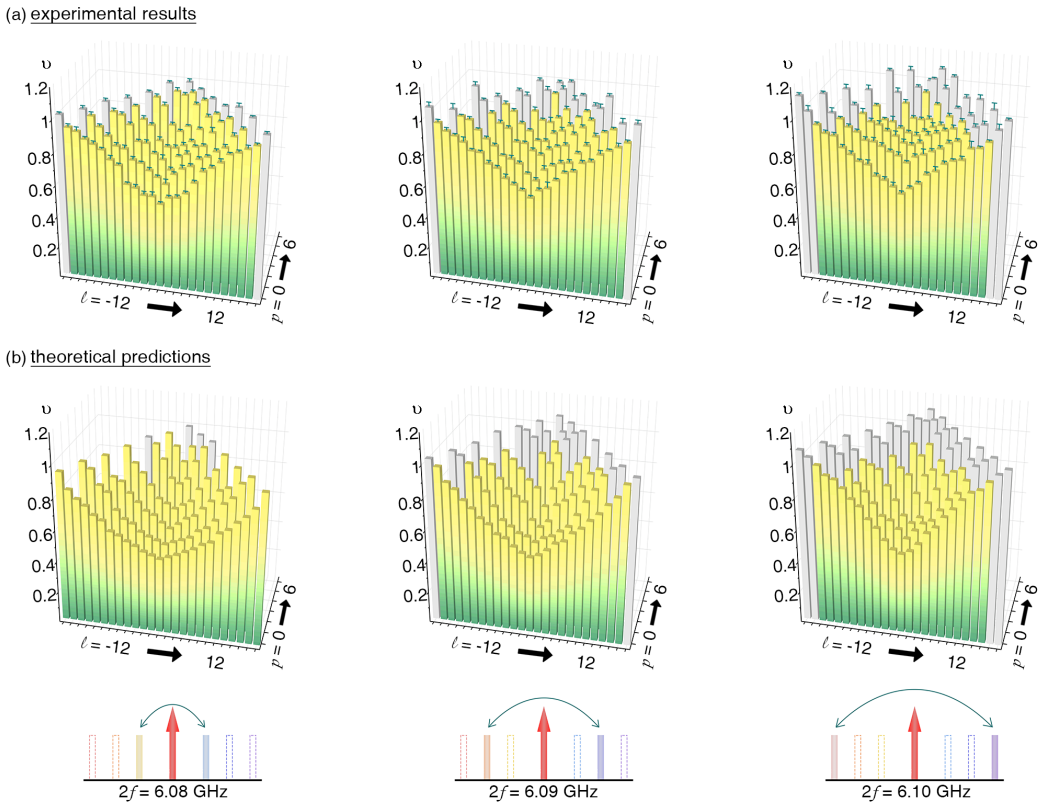

Fig S7 (a) Experimentally measured and (b) theoretically predicted smallest symplectic eigenvalue ν of the partially transposed covariance matrix. In each subfigure, the charts from left to right denote different frequency modes as indicated by the bottom. The error bars are obtained from the standard deviations of multiple repeated measurements.

Then we can construct the covariance matrix

$$\sigma_1 = \begin{bmatrix} \langle \hat{X}_a \hat{X}_a \rangle & \langle \hat{X}_a \hat{Y}_a \rangle & \langle \hat{X}_a \hat{X}_b \rangle & \langle \hat{X}_a \hat{Y}_b \rangle \\ \langle \hat{Y}_a \hat{X}_a \rangle & \langle \hat{Y}_a \hat{Y}_a \rangle & \langle \hat{Y}_a \hat{X}_b \rangle & \langle \hat{Y}_a \hat{Y}_b \rangle \\ \langle \hat{X}_b \hat{X}_a \rangle & \langle \hat{X}_b \hat{Y}_a \rangle & \langle \hat{X}_b \hat{X}_b \rangle & \langle \hat{X}_b \hat{Y}_b \rangle \\ \langle \hat{Y}_b \hat{X}_a \rangle & \langle \hat{Y}_b \hat{Y}_a \rangle & \langle \hat{Y}_b \hat{X}_b \rangle & \langle \hat{Y}_b \hat{Y}_b \rangle \end{bmatrix}. \tag{S37}$$

and calculate the smallest symplectic eigenvalue ν of the partially transposed covariance matrix to verify CV hyperentanglement.

According to the measured experimental parameters including intensity gains and visibilities

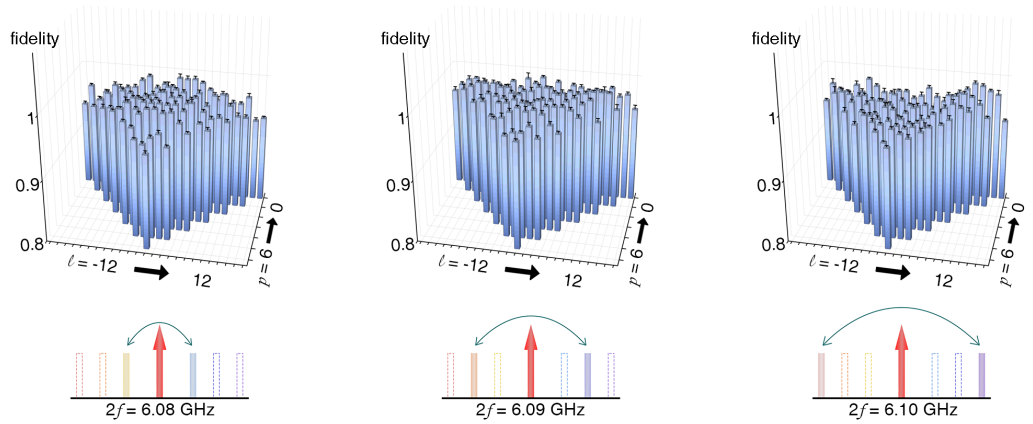

Fig S8 Fidelities between the theoretically predicted and experimentally generated hyperentangled states.

for different modes as shown in Fig. S5 above, all the theoretically predicted symplectic eigenvalue ν are shown in Fig. S7(b), which agree well with the corresponding experimental results as shown in Fig. S7(a).

The fidelities between the theoretically predicted and experimentally generated hyperentangled states can be calculated based on the quantum fidelity for arbitrary Gaussian states.[81] According to the theoretically predicted covariance matrix σ_1 (Eq. S37) and the experimentally measured covariance matrix σ_2, we can obtain the fidelity

$$F(\sigma_1,\sigma_2)=\frac{1}{\sqrt{\Gamma}+\sqrt{\Lambda}-\sqrt{(\sqrt{\Gamma}+\sqrt{\Lambda})^2-\Delta}}, \tag{S38}$$

where $\Gamma = 16\det(\Omega\sigma_1\Omega\sigma_2 - I_4/4)$, $\Lambda = 16\det(\sigma_1 + i\Omega/2)\det(\sigma_2 + i\Omega/2)$, $\Delta = \det(\sigma_1 + \sigma_2)$, $\Omega = \begin{pmatrix} 0 & 1 \\ -1 & 0 \end{pmatrix} \otimes I_2$, and I_n is the $n \times n$ identity matrix. The fidelities varying with ℓ, p, and f are shown in Fig. S8. These fidelities are all above 0.9, showing high similarity between the theoretically predicted and experimentally generated hyperentangled states.

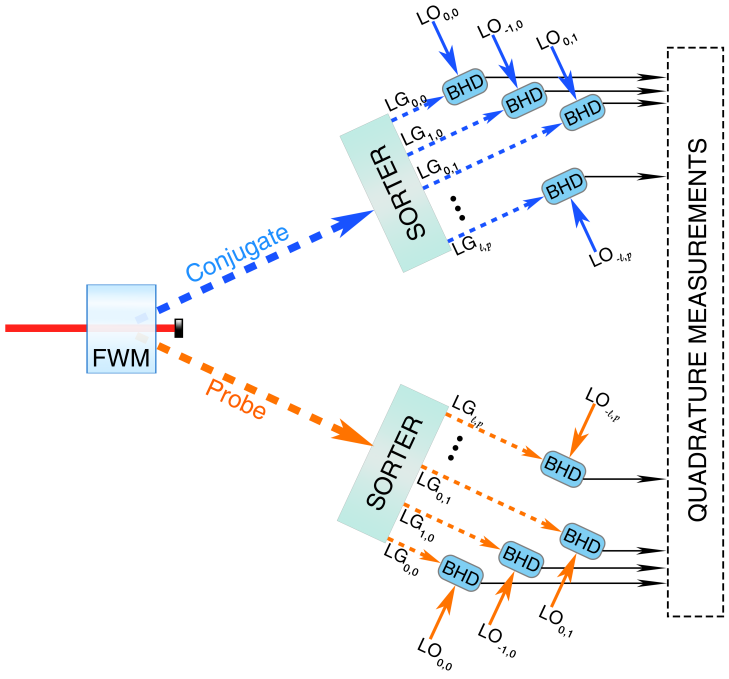

Fig S9 Separating hyperentangled modes based on LG mode sorter.

S9 Separating hyperentangled modes

By exploiting LG mode sorter and frequency filter cavity, all these hyperentangled modes can be spatially separated and individually accessed, making our system particularly useful for high-capacity parallel and multiple-DOF CV quantum communication.

There have been a series of studies on sorting LG modes according to their OAM and radial index.[58,59,73,74] A promising method is based on multi-plane light conversion (MPLC).[73,74] By employing wavefront modulation of multiple phase holograms, a beam containing multiple LG mode components can be decomposed into a grid of identical Gaussian spots each containing a single-mode LG component. In this way, sorting of OAM and radial modes can be easily implemented with high dimensionality. This method is efficient and can be integrated with our system as shown in Fig. S9.

Frequency filter cavity can be employed as frequency-dependent beam splitter to separate the

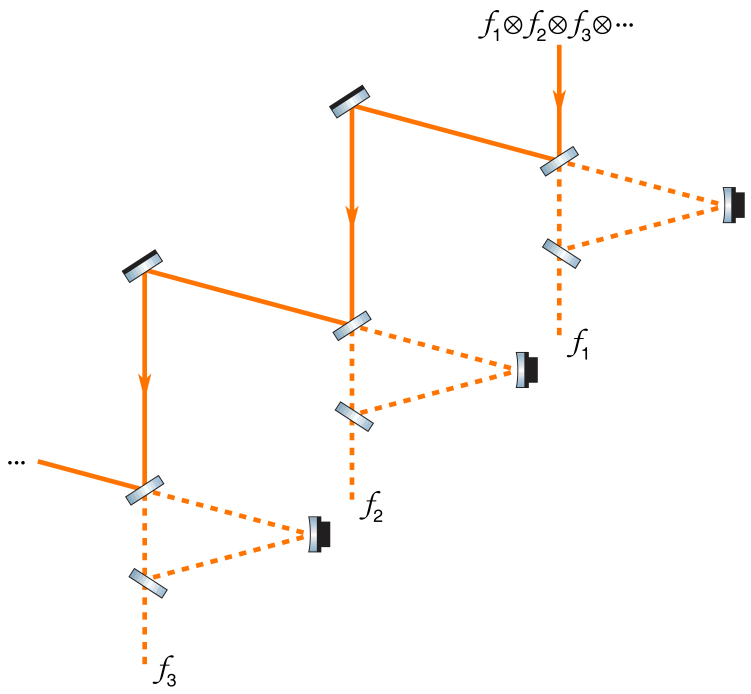

Fig S10 Separating hyperentangled modes based on frequency filter cavity.

frequency modes.[75] One such example is shown in Fig. S10. The ring filter cavity consists of three low loss mirrors, one is curved mirror, and two others are plane mirrors as the input-output coupling. When the ring filter cavity resonates with one of the frequency modes, it transmits this mode and reflects the rest. A cascade of several ring filter cavities can be employed to separate multiple frequency modes. Such method has been used to separate frequency multiplexed CV entangled states and demonstrate frequency multiplexing CV quantum dense coding.